

<https://helda.helsinki.fi>

Transfer standard for traceable dynamic calibration of stroboscopic scanning white light interferometer

Kassamakov, Ivan

2017-03-20

Kassamakov , I , Tureanu , A , Heikkinen , V & Haeggstrom , E 2017 , ' Transfer standard for traceable dynamic calibration of stroboscopic scanning white light interferometer ' , Applied Optics , vol. 56 , no. 9 , pp. 2483-2488 . <https://doi.org/10.1364/AO.56.002483>

<http://hdl.handle.net/10138/309160>

<https://doi.org/10.1364/AO.56.002483>

cc_by_nc

acceptedVersion

Downloaded from Helda, University of Helsinki institutional repository.

This is an electronic reprint of the original article.

This reprint may differ from the original in pagination and typographic detail.

Please cite the original version.

Transfer standard for traceable dynamic calibration of stroboscopic scanning white light interferometer

IVAN KASSAMAKOV^{1*}, ANCA TUREANU¹, VILLE HEIKKINEN² AND EDWARD HÆGGSTRÖM¹

¹Department of Physics, University of Helsinki, Helsinki FIN-00014, Finland

²VTT Technical Research Centre of Finland Ltd, Centre for Metrology MIKES, Espoo FIN- 02150, Finland

*Corresponding author: ivan.kassamakov@helsinki.fi

Received XX April 2015; revised XX Month, XXXX; accepted XX Month XXXX; posted XX Month XXXX (Doc. ID XXXXX); published XX Month XXXX

The reconstructed image of a moving sample shows always a distorted representation of reality. Therefore, one needs to calibrate, for example, out-of-plane nano-videos for quality control of Nano-Microelectromechanical systems (N-MEMS). Here we discuss how to calibrate and obtain confidence limits for Stroboscopic Scanning White Light Interferometry (SSWLI) data when there are differences in speed and amplitude across the field of view. Many N-MEMS devices rely on oscillating structures, consequently, one must calibrate movie recordings of these structures to have global standards and to allow inter-device comparison. We propose to use a quartz tuning fork driven off-resonance as a transfer standard. This approach allows a broad range of traceable frequencies and out-of-plane amplitudes to be introduced into selected parts of the field of view of the SSWLI device featuring similar optical surface properties to many N-MEMS devices, and without demanding an additional reference surface.

OCIS codes: (120.3940) Metrology; (120.4800) Optical standards and testing; (120.3180) Interferometry.

<http://dx.doi.org/10.1364/AO.99.099999>

1. INTRODUCTION

In Nano-Microelectromechanical systems modelling-based design and quality control (QC), “seeing is believing” and dynamic QC reveals features that cannot be observed in static measurements [1, 2]. Stroboscopic Scanning White Light Interferometry, a four dimensional (4D) camera, permits such advanced QC. Unfortunately the video camera “lies”, because the illumination and the motion of the object as well as its surface properties affect the way the sample is perceived. This is due to both optical and numerical image reconstruction reasons. One therefore needs to know how to calibrate the out-of-plane nano-videos of such N-MEMS structures. In practice one needs to solve the problem of how to calibrate and obtain confidence limits for SSWLI 4D data when there are differences in speed and amplitude across the field of view. This calibration problem relies on getting three things right: (i) identifying a transfer standard (TS) whose motion can be controlled and is known, (ii) making the TS motion traceable to the national standard, and (iii) finding a way to extract and implement the calibration parameters to raw 4D data (Fig. 1). Step (ii) is important since existing national standards are either quasi-dynamic [3] or mechanically narrow band (single frequency) dynamic [4].

The ability to do 4D calibration is valuable because most N-MEMS devices feature oscillating structures [5- 7]. By calibrating recorded repeatable movies of N-MEMS structures one can have global standards and inter-device comparison.

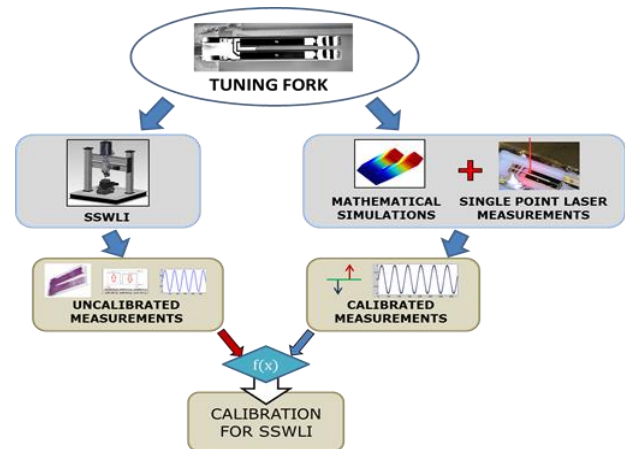


Fig. 1. Schematic description of 4D calibration.

There is a set of requirements such as - repeatable motion, size, and surface roughness which should be compatible with those present in N-MEMS, that a SSWLI-TS must fulfill [8]. The TS should feature no tall steps to minimize bat wing effects [8]. A quartz tuning fork (TF) driven off-resonance could potentially allow new calibration capability by permitting a broad range of traceable frequencies and out-of-plane amplitudes to be introduced into selected parts of the field-of-view of the SSWLI device. This solution has the extra advantage of requiring no additional reference surface. The solution is attractive because quartz tuning forks, a common frequency standard, feature well-known material properties as a function of ambient environmental parameters. The TF also possesses optical surface properties close to those of many N-MEMS devices.

The proposed solution is new because it permits calibration over a broad range of frequencies and most importantly over a broad continuous range of speeds across the field of view.

To perform the calibration, one could use a single point measuring device, e.g. a laser Doppler vibrometer (LDV), traceably linked to the national metrological standard, to measure the out-of-plane oscillation of the TF prongs. After that, the same motion under similar environmental (e.g. 21°C and 50% relative humidity) and drive-conditions should be measured with the SSWLI. To correct for speed differences across the SSWLI field of view we approximate the shape of the single prong by using the theoretical mode shape of the clamped free beam oscillating with the same frequency. The correction factor to be applied to the SSWLI data is different for each mode shape, each amplitude, and each position along the prong (Fig. 2).

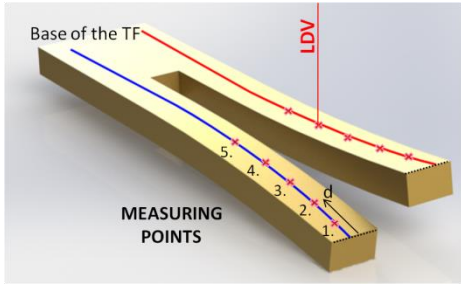


Figure 2: Quartz tuning fork driven in antisymmetric out-of-plane mode. Indicated are points that could be used for calibration with a laser Doppler vibrometer. Here d represents distance from the prong tip.

2. SSWLI ERROR ESTIMATION

SSWLI allows imaging oscillating samples when the device is equipped with pulsed illumination synchronized with the sample movement. In this way, to the image sensor – a CCD camera – the sample appears frozen and the measuring procedure can be done in the same way as in the static case. To image the sample in a different position a phase difference between the drive signal applied to the sample and the pulsed illumination is introduced. Theoretically, this issue has been considered in [9].

The general equation for the interference signal produced by a moving sample and stroboscopic illumination is:

$$I(\xi, \zeta) = \int_{-\infty}^{+\infty} u(K)q(K) \exp(i\zeta K) dK, \quad (1)$$

where the effect of sample motion is taken into account by the function:

$$u(K) = \frac{1}{\delta t} \int_{t_0 - \frac{\delta t}{2}}^{t_0 + \frac{\delta t}{2}} u(K)q(K) \exp(i\zeta K) dK, \quad (2)$$

with $\xi(t)$ parameterizing the oscillatory sample motion with frequency f and amplitude Λ :

$$\xi(t) = \Lambda \sin(2\pi f t). \quad (3)$$

Above, ζ represents the scan position, t_0 is the center of the stroboscopic pulse duration δt , and $q(K)$ describes the emission spectrum of the illumination source. The duty cycle is $D = f\delta t$.

A. Systematic measurement error estimation

Due to the stroboscopic illumination of the sample, a systematic measurement error emerges: the sample height is a function of the duty cycle. Naturally, the systematic error is a function of duty cycle. The measurement error due to sample motion at a certain t_0 is:

$$\Delta \xi(t_0) = \bar{\xi}(t_0) - \xi(t_0) = -\Lambda \left(1 - \frac{\sin(\pi D)}{\pi D} \right) \sin(2\pi f t_0), \quad (4)$$

where

$$\bar{\xi}(t_0) = \int_{t_0 - \frac{\delta t}{2}}^{t_0 + \frac{\delta t}{2}} \Lambda \sin(2\pi f t) dt. \quad (5)$$

As expected, the shorter the duty cycle, the smaller the systematic measurement error.

There are two important instances during the sinusoidal sample motion (we consider one period of motion, starting at $\xi = 0$):

- i) for $t_0 = 0$, the sample moves fast, but with constant speed. The measurement error (Eq. 4) is in this case zero, i.e. the average sample position during the illuminating pulse equals the exact sample position;
- ii) for $t_0 = T/4$ or $3T/4$, at the turning points of the oscillation, the sample moves very slowly, but the acceleration is maximum. In this case the measurement error is maximum, and Eq. (4) shows that the actual position is underestimated.

B. Restriction on duty cycle due to fringe contrast loss

The fringe contrast in the static case is described by the Fourier transform of the power spectrum emitted by the light source. When the sample moves (dynamic case), the power spectrum is additionally weighted by $u(K)$ in Eq. (1).

Even with a simple Gaussian power spectrum, the integrals are hard to calculate in closed analytic form. The general form of the signal, with a change of variables $\varphi = 2\pi f t$, is:

$$I(\xi) = (R + Z)I_w + 2\sqrt{RZ}I_w \frac{2}{2\pi D} * \text{Re} \int_{-\pi D}^{\pi D} \exp[2(\Delta K)^2 \xi^2(\varphi)] \exp[i2\bar{K}\xi(\varphi)] d\varphi, \quad (6)$$

where R and Z are the effective reflectivity (intensity) of the reference and object, respectively, I_w is the integral across the power spectrum of the light source, \bar{K} is the median and ΔK is the variance of the Gaussian distribution. The analysis of fringe contrast loss by de Groot is done using the approximation $\sin \varphi \sim \varphi$, which is justified only when the integration range in φ is less than 8° . This simplifying assumption means that πD in Eq. (6) is maximum 0.14 rad, which restricts the duty cycle to $< 2\%$. In this case the time-dependent optical path difference entering Eq. (6) is:

$$\xi(\varphi) = \Lambda \left(\frac{\sin(\pi D)}{\pi D} \sin(\varphi_0) + \varphi \cos(\varphi_0) \right), \quad \varphi_0 = 2\pi f t_0, \quad (7)$$

which simplifies the evaluation of the fringe contrast loss due to sample motion. Consequently, throughout this paper we consider duty cycles $D \leq 2\%$.

To apply the above general considerations to oscillating tuning forks, we review their mechanical oscillatory properties. To analyze the systematic measurement error, according to Eq. (4), one has to take into account the fact that the oscillation amplitude varies across the TF and find the explicit expression for the point-dependent amplitude. Also, one has to make sure that D is $\leq 2\%$ of the period of the vibration mode to be measured.

3. PROPERTIES OF AN OSCILLATING TUNING FORK

For convenience, we discuss four eigen modes of the TF. Two move in the horizontal plane (symmetric and anti phase) and two move out of that plane (symmetric and anti-phase). For calibration the preferred mode is the antisymmetric out-of-plane one, see Fig. 2. Tuning forks have been widely modeled in the literature by a single harmonic oscillator [10, 11]. At sufficiently small amplitudes ($\sin(x) \approx x$) the TF can be described as a harmonic oscillator subject to a harmonic driving force $F = F_0 \cos(\omega t)$ and a drag force with linear velocity dependence [10]. The equation of motion is:

$$\frac{d^2 x}{dt^2} + \gamma \frac{dx}{dt} + \frac{k}{m} x = \frac{F}{m} . \quad (8)$$

The four parameters are: mass m (of one prong), damping coefficient γ , spring constant k , and driving force amplitude F_0 . The mass and the damping coefficient depend on the medium surrounding the oscillating fork. The steady state solution of Eq. (8) is:

$$x(t) = x_a(\omega) \sin(\omega t) + x_d(\omega) \cos(\omega t), \quad (9)$$

where x_a and x_d parametrize the absorption and dispersion, respectively [10].

The general solution of Eq. (8) gives the mode shape of the beam/prong under different boundary conditions:

$$\phi(x) = A \sin x + B \cos x + C \sinh x + F \cosh x, \quad (10)$$

where A, B, C and F are integration constants. For a beam clamped at one end and free at the other end the mode shape is:

$$\phi(x) = \cosh(\lambda_i x/L) - \cos(\lambda_i x/L) - \sigma_i (\sinh(\lambda_i x/L) - \sin(\lambda_i x/L)), \quad (11)$$

where λ_i and σ_i are constants given by the boundary conditions, see [10]. Figure 3 shows the steady-state mode shape for the first three modes of the clamped – free beam [12].

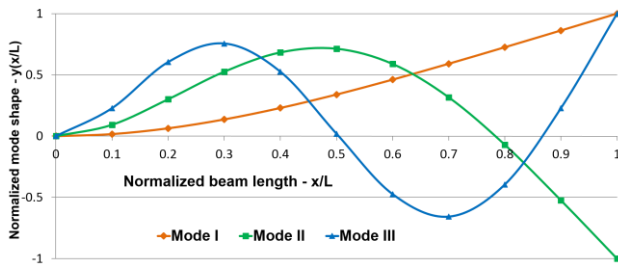


Figure 3. Steady-state mode shapes of first three modes of a clamped – free beam [12].

The corresponding time dependence of the i -th mode is $\sin 2\pi f_i t$ where:

$$f_i = \lambda_i^2 / 2\pi L^2 \left(\frac{EI}{m} \right)^{1/2}. \quad (12)$$

Here L is the length of the prong, E is the modulus of elasticity along the direction of oscillation, and I is the areal moment of inertia of the prong about its neutral axis [11].

4. METHODS

The theoretical model was tested by performing SSWLI and symmetric differential heterodyne laser interferometer (SDHLI) [13] measurements on a tuning fork at 5 positions along both prongs.

The measurements were done on a fork residing inside a closed IC package through the top glass surface of the device. This provides a stable pressure and humidity environment for the fork, but slightly decreases the measurement repeatability and limits the measurable area to within 2 mm from the free end of the fork. The laser interferometer limits the measurements to areas on the prong that are gold coated.

Both measurements relied on the visible edges of the gold coating and on the loss of signal at the end of the prong for position reference. In the SDHLI measurement only the gold areas gave a signal, whereas with SSWLI the edges of coated areas were seen as steps in the measured profile. The position along the prong of the SDHLI measurements was determined by the scale of a mechanical micropositioning stage with 5 μm division. The spot size of the SDHLI was reduced to 10 μm using a 50 mm focal length focusing lens. For SSWLI the effective pixel size of 2.96 μm (7.4 μm physical pixel size, 5x objective, 0.5x secondary lens) served as horizontal scale. The ambient temperature during the SDHLI measurements was 19.82 ± 0.04 °C whereas for SSWLI it was 23.3 ± 0.2 °C. The prong length determined using the 2D imaging mode of a Bruker ContourGT-K optical profiler (2.5x objective, 0.55x secondary lens) was 3060 ± 10 μm .

The measured peak to peak displacement is the average of measurements from the corresponding points on the two prongs. This approach was used since the prong movement was symmetric relative to the horizontal plane to within a precision of few nm and since the second prong moving in opposite phase could be used as reference surface for the SSWLI to cancel out drift.

5. EXPERIMENTAL RESULTS

The measurement results generated by both instruments corresponded to the theoretically predicted shape of mode 1 when the prong length was assumed to be 230 μm longer than the prong length measured from the separation point of the prongs to the tip of the prongs (Fig. 4). This result seems sensible since the base of the prongs can bend rotationally when the fork oscillates in the antiphase mode. The amplitude measured at point #3 was slightly off the predicted value in both instruments. This may be due to an uneven surface of the fork at this point (thin line of gold coating).

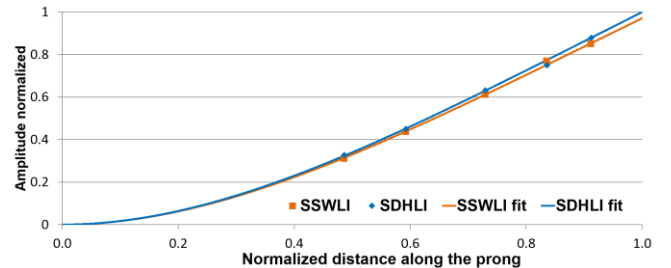


Figure 4. Measured shape of mode 1 in Fig. 3. Lines show fits using the theoretically predicted mode 1 shape for a 3290 μm long beam.

The measured displacements agreed with each other to within 3 %. A fit against a fork length of 3290 μm gives a peak-to-peak amplitude of 995 ± 7 nm for SSWLI and 1025 ± 8 nm for SDHLI at the fork end. The standard deviation of the vertical distance between the measured data points and the fit was 11.4 nm for SDHLI and 8.2 nm for SSWLI. The amplitude measured at 2750 μm from the prong base (point #3) deviated by ~ 20 nm from the predicted value in both instruments whereas the other measured data points were 3 nm or less from the predicted value in both instruments.

6. UNCERTAINTY ANALYSIS OF TFs MEASURED WITH SSWLI

We propose to use quartz TF working in anti-phase out of the plane mode as a transfer standard for SSWLI. Together with the benefits of using X-cut quartz as a TS material this choice removes the need for a specific reference surface. The fact that there is continuous displacement across the field of view allows efficient calibration of the SSWLI (one can rotate the fork as well as use different parts of the fork to calibrate different displacement amplitudes without changing the drive signal).

A. Pulse duration

The relation $D \leq 2\%$ must hold for every TF mode. We first analyze two independent prongs oscillating out-of-plane and in anti-phase (Fig. 2). The duty cycle is:

$$D = \delta t / T_i, \quad (13)$$

where T_i is the period of the i -th mode and δ is the stroboscopic pulse duration. By combining Eq. (12) and (13) the duty cycle necessary to image the i -th mode is:

$$D = \delta \lambda_i^2 / \left[2\pi L^2 \left(\frac{EI}{m} \right)^{1/2} \right] \quad (14)$$

For 2% duty cycle, the pulse duration necessary to image the i -th mode is:

$$(\delta)_i = 0.02 * 2\pi L^2 / \left[\lambda_i^2 \left(\frac{m}{EI} \right)^{1/2} \right] \quad (15)$$

B. Error estimation

We denote the transverse displacement (out-of-plane movement at position x) on the beam oscillating in mode i as:

$$\xi_i(x, t) = \phi_i(x) \sin(2\pi f_i t). \quad (16)$$

The systematic measurement error in z-direction due to sample motion, at a certain time coordinate for the pulse centered at t_0 , is:

$$\begin{aligned} \Delta \xi_i(x, t_0) &= \bar{\xi}_i(x, t_0) - \xi_i(x, t_0) = \\ &= -\phi_i(x) \left(1 - \frac{\sin(\pi D)}{\pi D} \right) \sin(2\pi f_i t_0). \end{aligned} \quad (17)$$

The absolute error along the z-axis when the oscillating object reaches its maximum deflection is

$$\Delta \xi_i(x) = -\phi_i(x) \left(1 - \frac{\sin(\pi D)}{\pi D} \right). \quad (18)$$

For every position x along the prong there is a certain underestimation of the maximum deflection, i.e. the error changes along the prongs. The same is true for the uncertainty in displacement estimate.

For $D = 2\%$, the relative bias estimate from Eq. (18) is:

$$\Delta \xi_i(x, D) / \phi_i(x) = 0.06\%. \quad (19)$$

Associated with any mean duty cycle \bar{D} there is a statistical uncertainty δD that affects the confidence limits of the measurement. Assuming x fixed and using the appropriate amplitude of the mode at that position, by the law of propagation of error, we have:

$$\delta(\Delta \xi_i(x, D)) = \left| \frac{d}{dD} (\Delta \xi_i(x, D)) \right|_D \delta D. \quad (20)$$

In our case, when $\Delta \xi_i(x, D)$ is given by Eq. (18):

$$\begin{aligned} \left| \frac{d}{dD} (\Delta \xi_i(x, D)) \right|_D &= \\ &= \left| \phi_i(x) \frac{1}{D} [\cos(\pi \bar{D}) - \text{sinc}(\pi \bar{D})] \right|. \end{aligned} \quad (21)$$

and:

$$\begin{aligned} \delta(\Delta \xi_i(x, D)) &= \\ &= \left| \phi_i(x) \frac{1}{D} [\cos(\pi \bar{D}) - \text{sinc}(\pi \bar{D})] \right|_D \frac{\delta D}{D} \end{aligned} \quad (22)$$

Obviously, this is a second order effect, since the quantity under the modulus sign is of the order of the magnitude of the bias, but it is multiplied by the relative error in \bar{D} . For a pulse duration of e.g. 5 ns, and an uncertainty in pulse duration of 0.1 ns, i.e. :

$$\frac{\delta D}{D} = 0.02, \quad (23)$$

we get:

$$\begin{aligned} \frac{\delta(\Delta \xi_i(x, D))}{\Delta \xi_i(x, D)} &= \\ &= \frac{[\cos(\pi \bar{D}) - \text{sinc}(\pi \bar{D})]}{1 - \text{sinc}(\pi \bar{D})} \frac{\delta D}{D} \approx 4\%. \end{aligned} \quad (24)$$

If we compare the uncertainty in bias estimate with the measured mode amplitude $\phi_i(x)$, the effect is practically negligible:

$$\frac{\delta(\Delta \xi_i(x, D))}{\phi_i(x)} = 0.0025\%. \quad (25)$$

C. Anti-phase prong movement

The TF is preferably operated in anti-phase mode in which both prongs oscillate out-of-plane (Fig. 2). In this case no reference surface is needed to measure the inter-prong distance along the z-axis (the top surface of the second prong serves as reference). The base of the TF may also serve as a reference if it fits into the field of view (Fig. 2). The error in this measurement again depends on the position on the prong (x) and is twice that calculated in the case of a single beam. Notably TFs,

do however, behave like a *pair of coupled beams whose dynamics strongly depends on the coupling* [11].

We initially modeled the TF prongs as two identical harmonic oscillators with mass m and elastic constants k . The coupling between the prongs could be modeled by a spring with elastic constant k_c . Within the harmonic approximation the natural modes that solve the equation system are: one in which the masses oscillate in-phase with identical amplitudes and another in which the masses oscillate in anti-phase with the same amplitudes. The mechanical coupling between the two harmonic oscillators breaks the degeneracy of the uncoupled identical oscillators generating two separate natural frequencies:

$$f_0^{in-phase} = \frac{\lambda_i^2}{2\pi} \sqrt{\frac{k}{m}}. \quad (26)$$

and

$$f_0^{anti-phase} = \frac{\lambda_i^2}{2\pi} \sqrt{\frac{k + 2k_c}{m}}, \quad (27)$$

where the superscript depicts the natural mode and the subscript "0" specifies that the two oscillators are identical as would be the case for a perfectly balanced TF. Based on Eqs. (26) and (27) the elastic constant of the coupling k_c can be expressed in terms of the elastic constant of one prong k and the natural frequencies of the two identical coupled

oscillators $f_0^{in-phase}$ and $f_0^{anti-phase}$ [11]:

$$k_c = \left[\left(\frac{f_0^{anti-phase}}{f_0^{in-phase}} \right)^2 - 1 \right]. \quad (28)$$

This points to a practical way of determining k_c . Equations (26) and (27) indicate that the *anti-phase frequency is higher than the in-phase one and this affects the error analysis*. For example, a commercial 32 kHz TF driven in out-of-plane mode

has $f_0^{anti-phase} \sim 6.14$ kHz and $f_0^{in-phase}$ frequency

~ 10.73 kHz. In this case $k_c = 2.05$. Assuming that the duration of the stroboscopic pulse δ is such that the duty cycle for the in-phase mode is 2% and if the frequency of the anti-phase mode is twice the frequency of the in-phase mode, then with the same δ , the duty cycle for the anti-phase mode is 4%. The corresponding relative errors for the in-phase and anti-phase mode, according to Eq. (18), are:

$$\frac{\delta(\Delta\xi_i(x, D^{in-phase}))}{\phi_i(x)} = 0.06\%$$

and

$$\frac{\delta(\Delta\xi_i(x, D^{anti-phase}))}{\phi_i(x)} = 0.26\%.$$

Even though the error is bigger for the anti-phase mode, the effect is still negligible when using a short duty cycle. The confidence limits are always small if de Groot's simple rule of thumb is used: keep the duty cycle of the light source $\leq 10\%$ of the period of the vibration mode to be measured.

7. DISCUSSION

We introduced a way to calibrate a SSWLI device used to obtain videos of oscillating N-MEMS structures. The approach employs a commercial quartz TF operating in out-of-plane anti-phase mode. The idea is that the mode-shapes are theoretically known and that the material properties of the specimen are rigidly controlled.

We derived theoretical estimates for measurement error and confidence limits for this estimate in a situation relevant to 4D microscopy. Focus was on bias induced by the sample motion. This has not been done before and represents an extension of de Groot's work [9]. Our approach is similar to what is done in current static calibration work (TS plus the idea of how to use it), but adapted to a new setting. One critique of the approach in a practical setting may be that we rely on the quartz TF behaving in a constant manner across a long measurement time since the LDV measures the motion on the tuning fork point-by-point. The second critique is that we have to move the TF since the approach doesn't allow us to calibrate all pixels in the field of view at once. The stability of the fork is again crucial, especially if the fork needs to be shifted and the calibration is performed in several discrete steps.

Fork stability could potentially be improved by frequency locking the fork to its peak frequency during calibrations. Another option may be to record possible frequency shifts during calibration. When the fork is run at constant frequency any disturbance to the fork that might shift its frequency would decrease the motion amplitude while moving the TS from calibration to possibly different and less controllable environments outside the calibration laboratory. Permanent changes to the TS can already now be checked by recalibrating the fork after use.

The practical feasibility of the proposed method as well as the theoretical predictions about fork movement shape was tested by performing SSWLI measurement along the length of an oscillating fork. These findings support the theoretical movement shape. The test also shows that the fork movement stays relatively stable during transport from fork calibration using laser interferometer to using it to calibrate SSWLI measurements.

The ability to calibrate 4D in a traceable manner opens up possibilities far beyond N-MEMS, e.g. the same approach can be used in bio-imaging.

8. CONCLUSION

We proposed a method where a quartz tuning fork serves as a traceable transfer standard to calibrate dynamic stroboscopic scanning white light interferometry. Experimental results using off the shelf forks indicate the practical feasibility of the proposed method.

More experimental work is needed to get the calibration uncertainty down to the nanometer level repeatability in SSWLI measurements.

Acknowledgment

This work was supported by EMRP NEW08 MetNEMS project and associate research excellence grant NEW08-REG3. The EMRP is jointly funded by the EMRP participating countries within EURAMET and the European Union.

The support of the Academy of Finland under the Project No. 136539 is gratefully acknowledged.

References

1. I. Kassamakov, K. Hanhijärvi, J. Aaltonen, L. Sainiemi, K. Grigoros, S. Franssila, and E. Hæggström, "Stroboscopic White Light Interferometry for Dynamic Characterization of Capacitive Pressure Sensors," Proceedings of Acoustics '08 Paris, France, 2523-2527 (2008).

2. D. Grigg, E. Felkel, J. Roth, X. C. de Lega, L. Deck, and P. J. de Groot, "Static and dynamic characterization of MEMS and MOEMS devices using optical interference microscopy," *Proc. SPIE* **5455**, MEMS, MOEMS, and Micromachining, 429-435 (2004).
3. G. Pedrini, J. Gaspar, M. E. Schmidt, I. Alekseenko, O. Paul, and W. Osten, "Measurement of nano/micro out-of-plane and in-plane displacements of micromechanical components by using digital holography and speckle interferometry," *Opt. Engin.* **50**(10), 101504-101513 (2011).
4. J. C. Marshall, D. L. Herman, P. T. Vernier, Member, D. L. DeVoe, and M. Gaitan, "Young's modulus measurements in standard IC CMOS processes using MEMS test structures", *IEEE El. Dev. Lett.*, **28**, (11), 960-963 (2007).
5. S. Petitgrand and A. Bosseboeuf, "Simultaneous mapping of phase and amplitude of MEMS vibrations by microscopic interferometry with stroboscopic illumination," *Proc. SPIE* **5145**, 33-44 (2003).
6. C. Giusca, L., R. K. Leach, and F. Helery, "Calibration of the scales of areal surface topography measuring instruments: Part 2 – Amplification coefficient, linearity and squareness," *Meas. Sc. and Techn.*, **23**, 065005-065015 (2012).
7. S. Petitgrand, R. Yahiaoui, K. Danaie, A. Bosseboeuf, and J.P. Gilles "3D measurement of micromechanical devices vibration mode shapes with a stroboscopic interferometric microscope," *Opt. and Lasers in Eng.*, **36**, 77–101 (2001).
8. J. Seppä, I. Kassamakov, V. Heikkinen, A. Nolvi, T. Paulin, A. Lassila, and E. Hæggsröm, "Quasidynamic calibration of stroboscopic scanning white light interferometer with a transfer standard", *Opt. Engin.*, **52**(12), 124104-1-124104-6 (2013).
9. P. de Groot, "Stroboscopic white light interference microscopy," *Appl. Optics* **45**, 5840-5844 (2006).
10. R. Blaauwgeers, M. Blazkova, M. Clovecko, V.B. Eltsov, R. de Graaf, J. Hosio, M. Krusius, D. Schmoranz, W. Schoepe, L. Skrbek, P. Skyba, R.E. Solntsev, and D.E. Zmeev, "Quartz tuning fork: thermometer, pressure and viscometer for helium liquids", *J. of Low Temp. Phys.*, **146**, 537-562 (2007).
11. A. Castellanos-Gomez, N. Agrit, and G. Rubio-Bollinger, "Dynamics of quartz tuning fork force sensors used in scanning probe microscopy," *Nanotechnology* **20**, 215502 (2009).
12. R. D. Blevins, "Formulas for natural frequency and mode shape", Krieger Pub Co, 492 (2001).
13. Traceable methods for vertical scale characterization of dynamic stroboscopic scanning white-light interferometer measurements, Heikkinen V, Kassamakov I, Seppä J, Paulin T, Nolvi A, Lassila A, Hæggsröm E., *Appl Opt.* **54**(35), 10397-403 (2015).